Clim. Past Discuss., 7, 841–886, 2011
www.clim-past-discuss.net/7/841/2011/
doi:10.5194/cpd-7-841-2011

Climate of the Past Discussions

Regional climate model experiments to investigate the Asian monsoon in the Late Miocene

H. Tang[1], **A. Micheels**[2,3], **J. Eronen**[1], **and M. Fortelius**[1]

[1]Department of Geosciences and Geography, P.O. Box 64, 00014 University of Helsinki, Finland
[2]Biodiversity and Climate Research Center (LOEWE BiK-F), Senckenberganlage 25, 60325 Frankfurt/Main, Germany
[3]Senckenberg Research Institute und Nature Museum, Senckenberganlage 25, 60325 Frankfurt/Main, Germany

Received: 2 February 2011 – Accepted: 16 February 2011 – Published: 1 March 2011

Correspondence to: H. Tang (hui.tang@helsinki.fi)

Published by Copernicus Publications on behalf of the European Geosciences Union.

Abstract

The Late Miocene (11.6–5.3 Ma) is a crucial period for the Asian monsoon evolution. However, the spatiotemporal changes of the Asian monsoon system in the Late Miocene are still ambiguous, and the mechanisms responsible for these changes are debated. Here, we present a simulation of the Asian monsoon climate (0 to 60° N and 50 to 140° E) in the Tortonian (11–7 Ma) using the regional climate model CCLM3.2. We employ relatively high spatial resolution (1° × 1°) and adapt the physical boundary conditions such as topography, land-sea distribution and vegetation in the regional model to represent the Late Miocene. As climatological forcing, the output of a Tortonian run with a fully-coupled atmosphere-ocean general circulation model is used. Our results show a stronger-than-present E-Asian winter monsoon wind in the Tortonian, as a result of the enhanced mid-latitude westerly wind of our global forcing and the lowered northern Tibetan Plateau in the regional model. The summer monsoon circulation is generally weakened in our regional Tortonian run compared to today. However, the changes of summer monsoon precipitation exhibit major regional differences. The precipitation decreases in N-China and N-India, but increases in S-China, the western coast and the southern tip of India. This can be attributed to the combined effect of both the regional topographical changes and the other forcings related to our global model. The spread of the dry summer conditions over N-China and NW-India further implies that the monsoonal climate may not be fully established over these regions in the Tortonain. Compared with the global model, the high resolution regional model highlights the spatial differences of the Asian monsoon climate in the Tortonian, and better characterizes the convective activity and its response to topographical changes. It therefore provides a useful and compared to global models complementary tool to improve our understanding of the Asian monsoon evolution in the Late Miocene.

CPD
7, 841–886, 2011

1 Introduction

The Late Miocene (11.6–5.3 Ma) is an important stage for the Asian monsoon evolution (e.g. Zachos et al., 2001). However, the change of the Asian monsoon climate in this period and its mechanism are still controversial (e.g. Wang et al., 2005; Molnar et al., 2010). Early evidence indicates the inception or a marked strengthening of the monsoon system in both S-Asia (e.g. Quade et al., 1989; Kroon et al., 1991) and E-Asia (e.g. Rea et al., 1998; An et al., 2001) at 8–7 Ma. This can be attributed to the surface uplift of the Tibetan Plateau (TP) (e.g. Ruddiman and Kutzbach, 1989; Kutzbach et al., 1993; An et al., 2001; Liu and Yin, 2002) and the retreat of the Paratethys (e.g. Ramstein et al., 1997; Fluteau et al., 1999).

More recent studies, however, challenge this idea, proposing the establishment of the monsoon climate in E-Asia and S-Asia much earlier than the Late Miocene (e.g. Guo et al., 2002; Sun and Wang, 2005; Clift et al., 2008). Instead of the weaker-than-present monsoon (or summer monsoon) in the Late Miocene suggested by earlier studies (e.g. Quade et al., 1989; An et al., 2001; Huang et al., 2007), a monsoon climate (or summer monsoon) similar to or even stronger than present is documented in recent studies (e.g. Dettman et al., 2001; Clift et al., 2008; Jiang and Ding, 2008). While the former result emphasizes the dominant influence of the regional tectonics, such as the TP uplift, on the monsoon changes in the Late Miocene, the latter one stresses the predominant impact of other forcings in the global climate system. For instance, it is suggested that the prevailing warmer global condition and less global ice volume in the Miocene would lead to a strong summer monsoon at that time (e.g. Jiang and Ding, 2008; Passey et al., 2009).

The complex spatiotemporal structure is an inherent feature of the modern Asian monsoon systems (e.g. Ding, 1992; Gadgil, 2003; Wang et al., 2008a). The response of the monsoon climate to different forcings (e.g. CO_2 concentration) varies from region to region (e.g. Zhu and Wang, 2002; Singh and Oh, 2007; Ashfaq et al., 2009). As the proxies from different localities accumulating, the complicated spatial pattern of the

CPD
7, 841–886, 2011

monsoon climate and the corresponding vegetation in the Late Miocene also start to emerge (e.g. Passey et al., 2009; Sanyal et al., 2010). Understanding such regional heterogeneity would be essential to unravel the discrepancies in the monsoon proxies and disentangle the mechanisms for the monsoon changes of this period.

Climate simulation with relatively thorough representation of global atmosphere and ocean conditions in the Late Miocene have been performed with different general circulation models (GCMs) (e.g. Dutton and Barron, 1997; Steppuhn et al., 2006, 2007; Micheels et al., 2007, 2010; Lunt et al., 2008). However, all these experiments use coarse spatial resolution, thus lack regional details over the Asian monsoon area. Furthermore, because of the coarse resolution, these experiments are not able to capture the influence of small-scale topography, which may exert substantial impact on the development of the Asian monsoon in the Late Miocene, such as the southern Tibet (e.g. Harris, 2006; Boos and Kuang, 2010). Compared to GCMs, regional climate models (RCMs) with high spatial resolution can resolve small-scale physical and dynamical processes, thus, perform better than GCMs in simulating the spatial patterns and the magnitude of the Asian monsoon precipitation (e.g. Gao et al., 2006, 2008). RCMs are also valuable tools for identifying the mechanisms associated with monsoonal circulation (e.g. Park and Hong, 2004; Singh and Oh, 2007). Some studies have applied RCMs to investigate the Asian monsoon in the mid-Holocene and the Last Glacial Maximum, and demonstrated better agreement of their RCM results with relevant geological evidence (Zheng et al., 2004; Ju et al., 2007). However, we are not aware of any regional climate model studies on the pre-Quaternary Asian monsoon climate.

In this study, the regional climate model – CCLM3.2 nested in one-way mode within a fully-coupled atmosphere-ocean general circulation model (AOGCM) (Micheels et al., 2010) is employed to simulate the mean state of the Asian monsoon climate in the Tortonian (11–7 Ma). We will firstly compare our regional model results with the driving global model and the monsoon proxies to demonstrate the regional pattern of the monsoon climate in the Tortonian and the adding values of our regional model results. Then, the effect of the Tortonian global forcing and regional boundary conditions (e.g.

CPD
7, 841–886, 2011

topography and vegetation) will be analyzed to further evaluate the contribution of different mechanisms to the monsoon evolution in the Late Miocene.

2 Model and model setup

2.1 The CLM model

The CLM is a non-hydrostatic RCM developed from the weather prediction Local Model of the German Weather Service (DWD) (Bohm et al., 2006). It has been used for present-day simulations and future climate projections in different regions (e.g. Christensen and Christensen, 2007; Jaeger et al., 2008; Rockel and Geyer, 2008) and can simulate the modern Asian monsoon precipitation patterns well compared to other RCMs (e.g. Rockel and Geyer, 2008; Dobler and Ahrens, 2010). In this study, we use the official model version CCLM 3.2 (available at: http://www.clm-community.eu), which has been evaluated and used for the CLM consortial runs (Hollweg et al., 2008). The model has a rotated geographical coordinate system with the vertical domain represented by a terrain-following hybrid coordinate system (η coordinate). In our experiments, we choose the leapfrog numerics (Skamarock and Klemp, 1992), the Tiedtke convection scheme (Tiedtke, 1989), the prognostic turbulent kinetic energy closure (Raschendorfer, 2001) and the TERRA-ML multi-layer soil model (Schrodin and Heise, 2002). More details on the model dynamics and physics can refer to the original documentations (Doms and Schattler, 2002; Doms et al., 2007).

2.2 Initial and lateral boundary forcing

As the lateral boundary forcing data for our regional model experiments, we use 6-hourly output from a present-day control run and a Tortonian run with AOGCM-COSMOS (ECHAM5/MPIOM) (Eronen et al., 2009; Micheels et al., 2010). These experiments with the global model are referred to as GCTRL and GTORT. The resolution

CPD
7, 841–886, 2011

of the spectral atmosphere general circulation model ECHAM5 is T31 (3.75°×3.75°) with 19 terrain-following vertical layers. The ocean circulation model MPIOM uses an Arakawa C-grid with an approximate resolution of 3° × 3° and the vertical domain is represented by 40 unevenly spaced levels. The setup design of GTORT is largely based on studies for the Late Miocene using the model version ECHAM4 coupled to a slab ocean model (Steppuhn et al., 2006, 2007; Micheels et al., 2007) (see also Table 1). Atmospheric CO_2 of GTORT is 360 ppm, which is the same as in GCTRL but also feasible for the Late Miocene (e.g. Pearson and Palmer, 2000; Micheels et al., 2009a). Because of the coarse model resolution, the palaeogeography is almost the same as today, but the Paratethys is included (based on Popov et al., 2004; Harzhauser and Piller, 2007) and the Panama Isthmus is open with a depth of 500 m (based on Collins et al., 1996). The palaeorography is generally reduced. For instance, the overall elevation of Tibet was reduced to about 70 to 80% of its present-day height (Fig. 1). Finally, surface parameters of the global model represent the Late Miocene vegetation, which is characterized by less desert and more forest cover than today (Micheels et al., 2007). For instance, boreal forest in GTORT covers the northern high latitudes, where there is tundra at present, and vegetation of North Africa is characterized by grassland to savanna instead of the modern Sahara desert.

Using the set of adapted Late Miocene boundary conditions, GTORT demonstrates a generally warmer (+1.5 °C) global condition compared to GCTRL. Global precipitation increases by +43 mm a^{-1} in GTORT due to the higher moisture loading in the atmosphere as a result of the higher surface temperature and greater evaporation over the ocean. Figure 2 illustrates the spatial distribution of the mean annual temperature and precipitation anomalies between GTORT and GCTRL. Primarily, higher latitudes are warmer than at present (Fig. 2a) and, hence, the meridional temperature gradient is weaker in GTORT. As a result of the open Panama Isthmus in GTORT, the northward heat transport in the Atlantic Ocean is weaker than in GCTRL. The reduced ocean heat transport explains the cooling in Northern Europe (Fig. 2a). Compensating for the weak ocean circulation, the westerlies intensify in GTORT (Fig. 2c, d). This is

CPD
7, 841–886, 2011

equivalent to an increased advection of moisture and, hence, increased precipitation in Europe (Fig. 2b) in GTORT compared to GCTRL. The presence of the Paratethys leads to a cooling trend (in summer) and increased rainfall nearby. North Africa gets significantly warmer (Fig. 2a) than in GCTRL because of the albedo effect. The "greening" of the Sahara in GTORT also enhances evapotranspiration and, thus, precipitation (Fig. 2b).

Over the Asian monsoon area, the lowering of the TP causes a strong warming of up to more than +10 °C in maximum. In winter, there is a clockwise wind field anomalies around the TP between GTORT and GCTRL (Fig. 2c). The northwesterly flow (i.e. the winter monsoon) over E-Asia is strengthened, while there is a stronger easterly flow in S-Asia in GTORT. The precipitation in E-Asia is weaker-than-present (Fig. 2b) because of the weaker summer monsoon circulation (Fig. 2d) as a result of the impact of lower TP in GTORT. The wind patterns of GTORT also represent a weaker-than-present Indian summer monsoon circulation (Fig. 2d). However, the precipitation strongly increases on the Indian subcontinent (Fig. 2b), which could be misinterpreted as a strengthening of the Indian summer monsoon. Such enhanced precipitation in GTORT is primarily driven by the higher Indian Ocean surface temperature, which leads to stronger evaporation and – although the atmospheric circulation is weaker – to a greater advection of moisture onto the Indian subcontinent (Micheels et al., 2010). In general, the results of GTORT compared to GCTRL are basically consistent to both fossil data and other Miocene model experiments (Eronen et al., 2009; Micheels et al., 2010). Therefore, we can use GCTRL and GTORT to force our regional climate model.

2.3 Experimental design

Our regional model domain covers the Asian monsoon area (0 to 60° N and 50 to 140° E) with a spatial resolution of 1° × 1°on the rotated model grid and 20 vertical levels. Two regional model experiments were performed at first: a present-day control run (CTRL) and a Tortonian run (TORT) (Table 2). For CTRL, we use the present-day global forcing (GCTRL) and the present-day physical boundary conditions (i.e.

CPD
7, 841–886, 2011

land-sea distribution, orography and vegetation) generated from WEB-PEP (version 0.74) (Smiatek et al., 2008).

For TORT, we use the Tortonian global forcing (GTORT). The configurations for the Tortonian physical boundary conditions in the regional model are also summarized in Table 1. As to the palaeorography, the high spatial resolution of the regional model allows us to modify the topography in more detail to better represent the Tortonian. We keep the elevations of the Himalayas and the southern TP as their present-day heights, but reduce the central and southeastern TP to 80% and the northeastern TP to 30% of their present-day heights (Fig. 3a, b). This is broadly consistent with the direct palaeoaltimetry studies (e.g. Rowley et al., 2001; Spicer et al., 2003; Rowley and Currie, 2006; Wang et al., 2008b) and the indirect tectonic (e.g. Coleman and Hodges, 1995; Blisniuk et al., 2001; Zheng et al., 2006; Liu-Zeng et al., 2008) and sedimentological inferences (e.g. Zheng et al., 2000). The general decrease of elevation from the south to the north of the TP agrees with the stepwise growth of the TP, such as that suggested by Tapponnier et al. (2001). For the topographic reliefs in other areas of our model domain, there are limited palaeoaltimetry studies, and most of them have gone through both pre-Tortonian and post-Tortonian surface uplift, such as the Tian Shan Mountain (e.g. Charreau et al., 2009) and the Zagros mountains (e.g. Lacombe et al., 2006). Therefore, we simply modify the elevations to 70–90% of their present-day heights in TORT (Fig. 3a, b). To be consistent, the roughness length of orography is also reduced proportionally to its surface elevation.

The modification of vegetation in TORT is mainly based on palaeobotanical data. As illustrated in Fig. 3, we replace the large desert area in C-Asia by herbaceous vegetation in TORT (based on Wolfe, 1985; Sun and Zhang, 2008; Sun et al., 2009). The vegetation on the southern TP is changed to mixed leaf trees (based on Liu, 1996; Tang and Shen, 1996). Evidence shows that the vegetation of the northern TP and the Loess Plateau underwent significant changes from forest to steppe in the Tortonian (at around 8 Ma) (e.g. Ma et al., 1998; Wang et al., 1999; Dong et al., 2006). Thus, we cover these areas with open forest, which acts as the transition zone between the forest

CPD
7, 841–886, 2011

in the east and the steppe in the west. E-China and S-Asia are dominated by forest in TORT (Fig. 3d). The distributions of broadleaved evergreen forest and subtropical forest in the Tortonian are similar to today (based on Zheng and Wang, 1994; Li and Zhang, 1998; Hoorn et al., 2000; Xia et al., 2009), but the temperate deciduous forest reaches farther north (based on Liu, 1998; Wang et al., 2001; Shu et al., 2008). The vegetation in TORT is in general agreement with the global vegetation reconstructions for the Late Miocene (e.g. François et al., 2006; Micheels et al., 2007).

The land-sea distribution in TORT is the same as that in CTRL, except the presence of the Paratethys. The extent of the Paratethys resembles to that in GTORT. The pCO_2 is 360 ppm for both CTRL and TORT, which is identical to our global forcing.

To further assess the contribution of the Tortonian regional boundary conditions (TORT-BC) and global forcing (i.e. GTORT) to the changes in TORT, two more sensitivity regional model experiments are carried out (Table 2), one of which uses the Tortonian global forcing (i.e. GTORT) but the present-day regional boundary conditions (refer to as TORTPD), one of which uses the present-day global forcing but TORT-BC (refer to as PDTORT). By subtracting the results of TORTPD and PDTORT runs by that of CTRL run (i.e. TORTPD minus CTRL and PDTORT minus CTRL), the effects of GTORT and TORT-BC can be obtained respectively. All the experiments were integrated for 10 years. The first year simulation is left for spin up and only the last 9-year results are used for analysis.

3 Results

3.1 Temperature

The annual average surface temperature increases significantly over the ocean and most of the continent in TORT, except C-Asia and N-India (Fig. 4a). The increase of surface temperature is most significant in the northern TP (more than +10 °C), Gobi Altai and Zagros Mountains where the surface elevations are greatly reduced. In C-Asia,

CPD
7, 841–886, 2011

the lower summer temperature but higher winter temperature (Fig. 4b,c) counteract each other on annual average and result in the little change of annual temperature in TORT (Fig. 4a). The insignificant change of temperature in N-India, however, persists throughout the year. Over the northern Asian continent, the increase of temperature is more pronounced in winter (Fig. 4b), while over the tropical ocean, the increase of temperature is more pronounced in summer (Fig. 4c). This suggests a reduced thermal contrast between land and ocean in both seasons.

3.2 Precipitation and evaporation

There is a general increase of precipitation over the mid-latitude areas (i.e. C-Asia and N-Asia) (especially in winter season) and most of the Ocean (especially in summer season) in TORT (Fig. 4d, e, f). The precipitation changes, however, show great regional difference in the monsoon regions. In S-Asia, the mean annual precipitation rate increases over the whole Arabian Sea, the western coast of India, the southern Bay of Bengal and the southern Indochina, while decreases over N-India, the northern Bay of Bengal and the northern Indochina in TORT (Fig. 4d). In E-Asia, there is an enhancement of annual precipitation over the Western North Pacific (WNP) and S-China, but a decline in the northern South China Sea (SCS) and N-China (Fig. 4d). The precipitation also intensifies over the southern TP but dampens in the northern TP. All these regional differences mainly occur in the summer season (Fig. 4f).

There is a stronger evaporation over the inland areas such as NW-China, C-Asia and N-India, probably related to the vegetation changes (e.g. from desert to grassland) in TORT (Fig. S1a in supplementary materials). The increase of evaporation is also observed over the whole Indian Ocean and the Japan Sea due to the higher sea surface temperature (SST). By contrast, the evaporation is subdued greatly over the modern Caspian Sea and Black Sea in TORT owing to the presence of the Paratethys and the great drop of summer temperature. The spatial pattern of the effective precipitation (precipitation minus evaporation) anomalies between TORT and CTRL is analogous to that of the precipitation changes (Fig. S1b in supplementary materials), except that the

CPD
7, 841–886, 2011

decrease of effective precipitation is more extensive due to the enhanced evaporation in TORT.

3.3 Air pressure and circulation

In winter, there is a stronger westerly wind over C-Asia in TORT (Fig. 5a). The Siberian-Mongolian High is weakened, but the northwesterly flow over E-China and easterly flow over N-India are strengthened (Fig. 5a). This indicates an intensified winter monsoon in TORT. The circulation changes are also visible at the mid-troposphere (at 500 hPa) in TORT, showing a generally invigorated westerly and northwesterly flow over C-Asia and E-China, but a slightly abated westerly over the southern slope of the TP (Fig. 5c). The Asian trough is a little shallower resulting in the significant southerly wind anomalies over NE-Asia (Fig. 5c).

In summer, a stronger westerly wind still prevails over C-Asia and N-Asia in TORT (Fig. 5b). The low pressure center in the N-Indian subcontinent is weakened (Fig. 5b). Consistently, a cyclonic wind anomaly appears around the Arabian Sea (Fig. 5b), reflecting a weaker summer monsoon wind (i.e. southwesterly flow) over most of the Arabian Sea and the Indian subcontinent in TORT. This also indicates a southward shift of the mean position of the tropical Convergence Zone (TCZ) (Fluteau et al., 1999), which explains the decrease of summer precipitation in the northern part of S-Asia, but the concurrent increase of precipitation in its southern part (Fig. 4f).

In E-Asia, there is a southward wind anomaly at 850 hPa, indicating a weakened summer monsoon in TORT (Fig. 5b). The significant westward wind anomaly over the SCS also suggests a reduced summer monsoon wind (i.e. southwesterly flow) in this area (Fig. 5b). As delineated by the contour of 58 000 $m^2 s^{-2}$ geopotential height at 500 hPa (Fig. 5d), the western North Pacific (WNP) Subtropical High, which covers the East China Sea and most of S-China in CTRL, retreats southward to the southern coast of China, and extends to the SCS and the Philippine Sea in TORT. This leads to the significant anticyclonic wind anomaly at both 500 hPa and 850 hPa over this region (Fig. 5b, d).

CPD
7, 841–886, 2011

The distribution of summer precipitation in E-Asia is closely related to the position and strength of the WNP Subtropical High (e.g. Liu et al., 2008; Chang et al., 2000). The summer rain belts are usually located in the southern flank (i.e. the WNP monsoon trough or WNP TCZ) and the northern flank (i.e. the subtropical front which is referred to as Mei-yu in China and Baiu in Japan) of the WNP Subtropical High. In contrast, the area dominated by the WNP Subtropical High is relatively dry. The southward displacement of the WNP Subtropical High and the associated rain belts (Fig. 5d) accounts for the increased summer precipitation in S-China but the reduced precipitation in N-China and the northern SCS in TORT (Fig. 4f).

3.4 Köppen classification

To further examine the changes of the monsoon climate regime in the Tortonain, we apply the Köppen climate classification (Kottek et al., 2006) to the output of TORT. The results are illustrated in Fig. 6. In N-China, there is an expansion of steppe climate (BS), replacing the winter dry climate (Dw) of today, due to the great decrease of precipitation in TORT. The desert climate (BW) in NW-China does not reach as far to the eastern Inner Mongolia as present day, but extends south- and southeast-ward to the northern TP and the western part of the Loess Plateau. By contrast, the desert climate (BW) in C-Asia shrinks greatly in TORT, replaced by the summer dry (Ds) and steppe (BS) climates. This is resulted from the increased precipitation (particularly the winter precipitation) in this area. In S-China, a large portion of the fully-humid climate (Cf) of the present disappears and becomes the winter dry climate (Cw), reflecting a stronger seasonality in TORT. The dominance of winter dry climates (Aw and Cw) in S-Asia and S-China implies that the monsoonal climate may have existed in the Tortonian and may have been even stronger than that at present in these areas. On the contrary, the monsoonal climate (as indicated by Dw) in N-China was still weak, and may not be fully established yet in the Tortonian.

CPD
7, 841–886, 2011

4 Discussion

4.1 Comparison with GTORT

The annual temperature changes in TORT are quite similar to that in GTORT (cf. Fig. 2a and Fig. 4a), depicting an extensive warmer condition in the Tortonian, but little change or slight cooling in C-Asia, N-India and the E-China Sea. The changes of precipitation, however, exhibit larger spatial difference in TORT than that in GTORT (cf. Fig. 2b and Fig. 4d), even though the large-scale trends of both experiments are consistent (Table 3). There is an out-of-phase change of precipitation between N-China and S-China, between SW-India and NE-India and also between the southern and northern TP in TORT, while there is only a generally decreased precipitation over E-China and increased precipitation over the whole India in GTORT. Little change of precipitation over TP is present in GTORT.

Such difference between TORT and GTORT does not reside in the horizontal wind field, which shows good agreement with each other (cf. Figs. 2c, d and 5a, b), but is manifested in the vertical motion. As illustrated in Fig. 7, the centre of the TCZ over the Indian Subcontinent, which is usually located at 20° N in the summer of present day (e.g. Goswami and Mohan, 2001; Gadgil, 2003), is well captured in our regional model but not in the global model. The rising motion is broadly strengthened over the whole Indian Subcontinent in GTORT (Fig. 7c, d). In contrast, TORT exhibits a weakened upward motion at 20° N, but a slightly intensified rising motion at 10° N (Fig. 7a, b), which suggests a southward shift of the TCZ. There is a generally dampened ascending motion over the TP in GTORT (Fig. 7c, d), while a strengthened rising motion over the southern TP and an enhanced sinking motion over the south and north of it are found in TORT (Fig. 7a, b). A finer structure of the changes in vertical motion is also observed to the north of the TP in TORT, such as the enhanced storm tracks at 50° N and the reduced topography-forced rising motion over the Tian Shan Mountain (Fig. 7a, b), all of which are missing in GTORT (Fig. 7c, d). These disparities in vertical wind velocity are closely linked to the convection and the topography described in

CPD
7, 841–886, 2011

the models. The better description of the regional structure of the vertical motion and the precipitation in TORT, hence, demonstrates the importance of using high-resolution model in characterizing the climate changes over the monsoon regions.

4.2 Comparison with monsoon proxies

4.2.1 Winter monsoon

Both TORT and GTORT display a stronger-than-present E-Asian winter monsoon wind (see WJ in Table 3). This is mainly associated with the changes in westerly flow on planetary scale rather than the surface pressure gradient between the Siberian High and the Aleutian Low on regional scale, which is weakened in both TORT and GTORT (see MO in Table 3) and would actually favour a weaker E-Asian winter monsoon wind. The importance of the westerlies in maintaining a strong winter monsoon wind in both GTORT and TORT, coincides with the studies by Ding et al. (1999) and Sun (2004), which emphasize the relevance of westerlies for dust transport and deposition on the Loess Plateau in the Late Miocene.

However, the stronger-than-present E-Asian winter monsoon wind in TORT and GTORT seems to be at odds with all the relevant proxies of this period (e.g. Rea et al., 1998; Guo et al., 2002; Jia et al., 2003; Wan et al., 2007). There was low dust accumulation rate over the western Loess Plateau (Fig. 8a), the North Pacific (with also the finer grain size of dust) (Fig. 8b) and the low black carbon accumulation rate over the northern SCS (Fig. 8c) in the Tortonian. This suggests that the E-Asian winter monsoon, the agent for dust transportation, was significantly weak in the Tortonian. Similar results can also be inferred by the lack of deposition of the wind origin "Red Clay" on the central Loess Plateau before 8–7 Ma (e.g. Sun et al., 1998; Qiang et al., 2001; Zhu et al., 2008).

The accumulation rate of the dust, which most of the winter monsoon proxies rely on, is not only governed by the strength of the winter monsoon wind but also controlled by its supply which can be affected by the vegetation in the dust source regions (Rea

CPD
7, 841–886, 2011

et al., 1998; Jia et al., 2003). Our results indicate an intensified mid-latitude precipitation, particularly in winter time (Fig. 4e), and an alleviated arid condition between 50° N to 40° N of the Asian continent in the Tortonian (Fig. 6b). This may suppress the dust supply and lead to the low dust accumulation rate and grain size found in the ODP site 885/886 (44.7° N, 168.3° W) from North Pacific (Fig. 8b). On the other hand, the Loess Plateau, from which most of the dust records were retrieved, are mainly covered by desert or dry steppe climate in the Tortonian (Fig. 6b). This may facilitate the mobilization of the dust more than the capture of the dust (e.g. the wet deposition) (Yue et al., 2009), hence, result in the low dust deposition rate at that time. As indicated by our model result, the surface conditions (e.g. the vegetation and the topography) probably play a more important role than the winter monsoon wind in controlling the dust accumulation in the Tortonian.

4.2.2 E-Asian summer monsoon

Both TORT and GTORT reveal a weaker summer monsoon wind and a drier-than-present condition of N-China in the Tortonian (Fig. 2b, d and Fig. 4f, 5b). This is consistent with the hypsodonty of the fossil mammal teeth, which documents less precipitation (higher hypsodonty) of N-China in most of the Tortonian (11–8 Ma) than present day (Fortelius et al., 2002; Eronen et al., 2010) (Fig. 9a), but contradicts to the pollen studies by Jiang and Ding (2008, 2009) (Fig. 8d), which report a moisture condition in the Tortonian similar to or moister than that of the present. Passey et al. (2009) shows the expansion of C_4 plants over N-China after 7 Ma (Fig. 8e), and regarded such changes as the shift of the semi-humid climate band which favours the growth of C_4 plants (i.e. steppe forest) into N-China. The few occurrences of C_4 plants before 7 Ma can be attributed to the either too dry or too humid condition in N-China (Passey et al., 2009). Our results imply that it is probably the drier condition that inhibits the growth of C_4 plants in N-China in the Tortonian. The dominance of the arid climates over N-China in TORT (Fig. 6b) demonstrates a more zonal distributed (planetary-like) mid-latitude aridity in the Tortonian. This confirms the studies by Liu et al. (2009, 2010)

CPD
7, 841–886, 2011

based on the mammal and plant fossil records, and supports the onset of summer monsoon in N-China in the Late Miocene (e.g. An et al., 2001) rather than the Early Miocene (e.g. Sun and Wang, 2005; Guo et al., 2008).

In S-China, both TORT and GTORT display a strengthened summer monsoon precipitation. However, on annual average, the precipitation decreases in GTORT (Fig. 2b), but increases in TORT (Fig. 4d). The results of TORT are in better agreement with the chemical weathering index retrieved from the northern SCS (Fig. 8f), which reflects a stronger runoff (thus precipitation) of the drainage of the Pearl river in the Tortonian than the subsequent periods. The higher monsoon precipitation of S-China has been intuitively regarded as an indication of strong E-Asian summer monsoon in the Miocene (e.g. Clift et al., 2008; Steinke et al., 2010) (Fig. 8f), which conflicts with the weak E-Asian summer monsoon evidenced in the proxies from N-China (e.g. An et al., 2001; Fortelius et al., 2002; Passey et al., 2009) (Fig. 8e). However, as illustrated in TORT, the precipitation changes in S-China and N-China are out-of-phase. Therefore, the seemingly contradicted records from S-China and N-China are actually concordant with each other, and both point to a weak E-Asian summer monsoon in the Tortonian according to the definition of its strength (see more discussion on the definition of the E-Asian summer monsoon strength in Wang et al., 2008a). There is an marked decline of the monsoon precipitation of S-China at the end of the Tortonian (Clift et al., 2008; Steinke et al., 2010) (Fig. 8f), coinciding with the significant increase of monsoon precipitation in N-China (e.g. Fortelius et al., 2002; Kaakinen et al., 2006; Passey et al., 2009) (Fig. 8e). This further corroborates the existence of the out-of-phase precipitation changes between N-China and S-China and provides a coherent evidence for the strengthening of the E-Asian summer monsoon at 8–7 Ma.

4.2.3 Indian summer monsoon

Both TORT and GTORT suggest a weakened Indian summer monsoon circulation (see WY in Table 3 and Fig. 5b). This agrees well with the weak summer monsoon-driven upwelling over the western Arabian sea in the Tortonian (Kroon et al., 1991; Huang

CPD
7, 841–886, 2011

et al., 2007) (Fig. 8i). However, it is still elusive on the moisture condition over the continent of S-Asia, which is closely linked to the summer monsoon precipitation in the Tortonian. GTORT reveals a fully humid condition over the whole Indian Subcontinent (Fig. 2b). This sides with the studies on pollen assemblages (Fig. 8h) and $\delta^{18}O$ of bivalve shells in Nepal (Hoorn et al., 2000; Dettman et al., 2001) and the low hypsodonty of the mammal fossil teeth (Fig. 9a). Similar results are also discovered in the record from the southern tip of the Indian Peninsula (Armstrong-Altrin et al., 2009) and manifested by the higher chemical weathering and physical erosion of the Himalayas and the foreland basins in the Tortonian (Derry and FranceLanord, 1996; Clift et al., 2008).

TORT also supports the wetter conditions in the southern Indian and the southern TP (Fig. 4d), but indicates a drier condition over the N-Indian Subcontinent. This disagrees with the proxies from C-Nepal (Hoorn et al., 2000; Dettman et al., 2001) (Fig. 8h) , but is in better accordance with the $\delta^{13}C$ record of the pedogenic carbonate from N-Pakistan (Fig. 8g) (Quade et al., 1989) and the western Himalayan foreland basin (Sanyal et al., 2010), which reflect a weak summer monsoon precipitation before 8–7 Ma and a striking enhancement afterwards. Note that although the summer precipitation is reduced over the N-Indian subcontinent in TORT, the Köppen classification reveals that the monsoonal climate (Cwa) may have existed in most of this area in the Tortonian (Fig. 6b). This concords with the evidence from C-Nepal (Dettman et al., 2001) and SW-China (Xia et al., 2009; Jacques et al., 2010). Whereas, a summer dry climate (Csa) covers the foreland basin of the western Himalayas in TORT (Fig. 6b), indicating the emergence of the monsoonal climate of this region is probably later than the Tortonian and also than that in the rest of the Indian Subcontinent. This further comfirms the results of Quade et al. (1989) and Sanyal et al. (2010) and implies a spatial difference in the development of the Indian monsoon in the Tortonian.

4.2.4 Aridity in C-Asia

A relatively humid condition of C-Asia is found in our results, which concurs with pollen study by Sun and Zhang (2008) and the low hypsodonty of this period (Fig. 9a). In

CPD
7, 841–886, 2011

contrast, the arid condition over NW-China is already present in the Tortonian (Fig. 6b). This contradicts to Ma et al. (1998, 2005) and Sun et al. (2009) which claims a humid condition of NW-China in the Tortonian and the initiation of the desert around 8-7 Ma, but is in agreement with Pettke et al. (2000), which argues that the desert in NW-China may have been formed in the Tortonian. The $\delta^{18}O$ records from Linxia Basin (Dettman et al., 2003) and the high hypsodonty (Fig. 9a) also support the presence of dry climate over NW-China already in the Tortonian.

4.3 Influence of global forcing and regional boundary conditions

The climate changes in TORT are the combined effect of both its global forcing (i.e. GTORT) and regional boundary conditions (TORT-BC). Disentangling the changes related to GTORT (i.e. TORTPD minus CTRL) and TORT-BC (i.e. PDTORT minus CTRL) would provide a useful guidance to the mechanisms responsible for the monsoon changes. Owing to the fact that the regional vegetation changes have minor impact on most of the climate variables in TORT (data no shown), the effect of TORT-BC can be simply regarded as the response to the regional orographic changes. In contrast, the effect of GTORT is more associated with the changes in global climate system which may be far away from our regional domain.

The overall warmer condition in TORT is largely due to GTORT (Fig. S2 in the supplementary materials). The contribution of TORT-BC to the warmer TORT only restrict to the areas with reduced elevation. And TORT-BC even has cooling effect over N-India. This counteracts the warming effect of GTORT, leading to little change of temperature over this area in TORT (Fig. 4a). The warmer winter but cooler summer of C-Asia in TORT is affected by both GTORT and TORT-BC (Fig. S2 in the supplementary materials), in which the presence of the Paratethys acts as a temperature buffer to its surrounding area owing to its greater heat capacity (Ramstein et al., 1997; Fluteau et al., 1999).

Both GTORT and TORT-BC give rise to the stronger E-Asian winter monsoon wind in TORT (see WJ in Table 3). As illustrated in Fig. 10a, GTORT is only responsible

CPD
7, 841–886, 2011

for the strengthening of the winter monsoon wind in N-China. This is related to the enhancement of the westerly over C- and N-Asia in GTORT, which is shown in Micheels et al. (2010) to be induced by the weakened Atlantic thermohaline circulation as the result of the opening of the Panama Isthmus. By comparison, TORT-BC does not only contribute to the stronger winter monsoon wind in N-China, but also strengthens the winter monsoon wind in S-China and N-India (Fig. 10c). This can be attributed to the effect of the lower northern TP that allows more westerly flowing through the northern TP to N-China, while diminishes the westerly flow south of the TP (Fig. 10c). The enhanced cold advection from E-Asia to N-India as a result of TORT-BC may account for the decrease of winter temperature in PDTORT (Fig. S2 in the supplementary materials).

GTORT exerts extensive impact on both the large-scale and the regional pattern of the summer monsoon circulation and precipitation changes in TORT. The precipitation over most of S-Asia is intensified by GTORT (see EIMR in Table 3 and Fig. 11c) owing to its higher SST of the Indian Ocean which may relates to the opening of the Indonesian Seaway in GTORT (Cane and Molnar, 2001). Both the S-Asian and E-Asian summer monsoon circulation are, however, weakened largely by GTORT (see WY in Table 3 and Fig. 10b), in which the dampened summer monsoon circulation is primarily ascribed to the combined effect of the lower whole TP and the presence of the Paratethys (Micheels et al., 2010) (Fig. 1). In addition, other mechanisms may also play a role, such as the reduced orography in E-Africa (Chakraborty et al., 2002) and the grassland cover of Sahara in GTORT (Micheels et al., 2009b). The sharpened difference in the strength of southerly wind between S-China and N-China in TORT is largely caused by GTORT (see WYF in Table 3 and Fig. 10b). It is, therefore, GTORT which brings about the regional difference of the precipitation changes between N- and S-China in TORT (Fig. 4f). This further proves that the regional difference is an inherent feature of the Asian monsoon system, which is not visible in GTORT simply because of its coarse resolution.

CPD
7, 841–886, 2011

Compared to GTORT, the contribution of TORT-BC to the summer monsoon changes in TORT is limited. There is an abated summer monsoon wind (see WN in Table 3 and Fig. 10d) and a distinct decrease of precipitation accordingly in N-China (Fig. 11f) due to TORT-BC. This indicates the strong influence of the lower northern TP on the summer monsoon strength over N-China, which is in concert with the global model study by Boos and Kuang (2010). TORT-BC has little influence on the summer monsoon in S-Asia (see EIMR and WY in Table 3 and Fig. 10d, 11f). This lends support to the idea that the southern TP alone is sufficient to maintain a summer monsoon of present-day strength in S-Asia (Boos and Kuang, 2010). There is only a small weakening of the southwesterly in W-India and Pakistan induced by the TORT-BC (Fig. 10d). This can be attributed to the lower Zagros Mountains (70% of the present-day height) (Fig. 3b) that allows the intrusion of mid-latitude dry air to N-India, hence delays the seasonal onset of the summer monsoon (Chakraborty et al., 2002). TORT-BC also plays an important role in the precipitation changes over TP and NE-Asia (Fig. 11f), suggesting that the precipitation changes in these areas can be highly sensitive and indicative to the regional topographic changes.

Our results emphasize the influence of both the global climate and the regional tectonic changes on the monsoon evolution in the Tortonian. It is probably the combined effect of both that prevent the monsoonal climate pattern forming in N-China in the Tortonian (Fig. 6b). This is in contrast with the model studies by Zhang et al. (2007a,b) which suggest the transition of palaeo-environment in N-China from planetary-like to monsoon-like pattern in the early Miocene with only the effect of the regional tectonic changes being considered. It has been proposed that the warmer condition over the oceans and the high-latitudes in the Late Miocene or before, would be able to maintain a strong summer monsoon (precipitation), while the TP may play a secondary role supposing it has uplifted to a substantial height at that time (e.g. Clift et al., 2008; Jiang and Ding, 2008; Passey et al., 2009). This, however, is not justified by our model results at least for the Tortonian. The precipitation does increase on our domain average in TORT due to the warmer conditions, but such increase is quite unevenly distributed

CPD
7, 841–886, 2011

and mostly occurs in the ocean (Table 3) and the maritime continent (Fig. 4d). Although the elevation of the orography prescribed in TORT (Fig. 3b) may represent the highest scenario in the Tortonian, it still noticeably weakens the monsoon circulation in N-China and NW-India. This limits the penetration of moisture from the ocean to the continent (Fig. 10d), and results in a drier condition in these areas (Fig. 11f). The competing effects of the lower TP (weakening summer monsoon circulation) and the warmer ocean (enhancing moisture supply), further amplify the regional contrast of the monsoon climate in the Tortonian, which is inherent in the Asian monsoon system.

5 Conclusions

In summary, our regional model simulation yields a Tortonian Asian monsoon climate that is comparable to our global forcing model on large-scale patterns, but highlights the regional difference of the monsoon climate which resolves some apparent contradictions in the monsoon proxies of this period. Our results suggest a stronger E-Asian winter monsoon wind in the Tortonian as a result of the strengthened global westerly flow and the lower northern TP. The summer monsoon circulation is generally weaker in the Tortonian, associated with the decrease of monsoon precipitation in N-China and N-India, but the increase of precipitation over S-China and S-India. This implies the earlier presence of strong monsoonal climate in S-India and S-China, but a later onset of monsoonal climate in N-China and NW-India in the Tortonain. While the changes of summer monsoon over S-Asia and S-China are mainly controlled by our global forcing, the summer monsoon over N-China is more susceptible to the regional orographic changes (i.e. lower northern TP). The different effect of the changes in global climate and the regional tectonics is particularly pivotal to the maintaining of the regional heterogeneity of the monsoon climate in the Tortonian.

CPD
7, 841–886, 2011

Supplementary material related to this article is available online at: http://www.clim-past-discuss.net/7/841/2011/cpd-7-841-2011-supplement.zip.

Acknowledgements. We thank the Ella and Georg Ehrnrooth foundation for project funding. This work was also financially supported by the Deutsche Forschungsgemeinschaft DFG within the project FOR 1070 and the federal state Hessen (Germany) within the LOEWE initiative, and is a contribution to the NECLIME framework. We acknowledge the model support of the CLM community especially from Andreas Will, Burkhardt Rockel and Hans-Jürgen Panitz. Our model experiments have been performed at the Center for Scientific Computing (CSC) in Espoo (Finland) with special technical support from Juha Lento and Tommi Bergman. We would also like to thank Bodo Ahrens, Andreas Dobler, Mark Herrmann, Liu Liping, Anu Kaakinen and Zhou Liping for comments, help and fruitful discussions.

References

An, Z. S., Kutzbach, J. E., Prell, W. L., and Porter, S. C.: Evolution of Asian monsoons and phased uplift of the Himalayan Tibetan plateau since Late Miocene times, Nature, 411, 62–66, 2001. 843, 856

Armstrong-Altrin, J. S., Lee, Y. I., Verma, S. P., and Worden, R. H.: Carbon, oxygen, and strontium isotope geochemistry of carbonate rocks of the upper Miocene Kudankulam Formation, southern India: Implications for paleoenvironment and diagenesis, Chemie Der Erde-Geochemistry, 69, 45–60, 2009. 857

Ashfaq, M., Shi, Y., Tung, W. W., Trapp, R. J., Gao, X. J., Pal, J. S., and Diffenbaugh, N. S.: Suppression of south Asian summer monsoon precipitation in the 21st century, Geophys. Res. Lett., 36, L01704, doi:10.1029/2008GL036500, 2009. 843

Beck, C., Grieser, J., and Rudolf, B.: A new monthly precipitation climatology for the global land areas for the period 1951 to 2000, Climate status report 2004, German Weather Service, Offenbach, Germany, 2005. 881

Blisniuk, P. M., Hacker, B. R., Glodny, J., Ratschbacher, L., Bi, S. W., Wu, Z. H., McWilliams, M. O., and Calvert, A.: Normal faulting in central Tibet since at least 13.5 Myr ago, Nature, 412, 628–632, 2001. 848

CPD
7, 841–886, 2011

Boos, W. R. and Kuang, Z. M.: Dominant control of the South Asian monsoon by orographic insulation versus plateau heating, Nature, 436, 218–223, 2010. 844, 860
Cane, M. A. and Molnar, P.: Closing of the Indonesian seaway as a precursor to east African aridircation around 3–4 million years ago, Nature, 411, 157–162, 2001. 859
Chakraborty, A., Nanjundiah, R. S., and Srinivasan, J.: Role of Asian and African orography in Indian summer monsoon, Geophys. Res. Lett., 29, 1989, doi:10.1029/2002GL015522, 2002. 859, 860
Chang, C. P., Zhang, Y. S., and Li, T.: Interannual and interdecadal variations of the East Asian summer monsoon and tropical Pacific SSTs. Part I: Roles of the subtropical ridge, J. Climate, 13, 4310–4325, 2000. 852
Charreau, J., Chen, Y., Gilder, S., Barrier, L., Dominguez, S., Augier, R., Sen, S., Avouac, J. P., Gallaud, A., Graveleau, F., and Wang, Q. C.: Neogene uplift of the Tian Shan Mountains observed in the magnetic record of the Jingou River section (northwest China), Tectonics, 28, TC2008, doi:10.1029/2007TC002137, 2009. 848
Christensen, J. H. and Christensen, O. B.: A summary of the PRUDENCE model projections of changes in European climate by the end of this century, Climatic Change, 81, 7–30, 2007. 845
Clift, P. D., Hodges, K. V., Heslop, D., Hannigan, R., Van Long, H., and Calves, G.: Correlation of Himalayan exhumation rates and Asian monsoon intensity, Nat. Geosci., 1, 875–880, 2008. 843, 856, 857, 860, 883
Coleman, M. and Hodges, K.: Evidence for Tibetan Plateau Uplift before 14-Myr Ago from a New Minimum Age for East-West Extension, Nature, 374, 49–52, 1995. 848
Collins, L. S., Coates, A. G., Berggren, W. A., Aubry, M. P., and Zhang, J. J.: The late Miocene Panama isthmian strait, Geology, 24, 687–690, 1996. 846
Derry, L. A. and FranceLanord, C.: Neogene Himalayan weathering history and river Sr-87/Sr-86: Impact on the marine Sr record, Earth Planet. Sci. Lett., 142, 59–74, 1996. 857
Dettman, D. L., Kohn, M. J., Quade, J., Ryerson, F. J., Ojha, T. P., and Hamidullah, S.: Seasonal stable isotope evidence for a strong Asian monsoon throughout the past 10.7 m.y, Geology, 29, 31–34, 2001. 843, 857
Dettman, D. L., Fang, X. M., Garzione, C. N., and Li, J. J.: Uplift-driven climate change at 12 Ma: a long $\delta^{18}O$ record from the NE margin of the Tibetan plateau, Earth Planet. Sci. Lett., 214, 267–277, 2003. 858
Ding, Y. H.: Summer Monsoon Rainfalls in China, Journal of the Meteorological Society of

CPD
7, 841–886, 2011

Japan, 70, 373–396, 1992. 843
Ding, Z. L., Xiong, S. F., Sun, J. M., Yang, S. L., Gu, Z. Y., and Liu, T. S.: Pedostratigraphy and paleomagnetism of a similar to 7.0 Ma eolian loess-red clay sequence at Lingtai, Loess Plateau, north-central China and the implications for paleomonsoon evolution, Palaeogeogr. Palaeocl., 152, 49–66, 1999. 854
Dobler, A. and Ahrens, B.: Analysis of the Indian summer monsoon system in the regional climate model COSMO-CLM, J. Geophys. Res.-Atmos., 115, D16101, doi:10.1029/2009JD013497, 2010. 845
Doms, G. and Schattler, U.: A Description of the nonhydrostatic regional model LM (Part I): dynamics and numerics, available at: http://www.cosmo-model.org/, 2002. 845
Doms, G., Forstner, J., Heis, E., Herzog, H. J., Raschendorfer, M., Reinhardt, T., Ritter, B., Schrodin, R., Schulz, J. P., and Vogel, G.: A description of nonhydrostatic regional model LM (Part II): physical parameterization, available at: http://www.cosmo-model.org/, 2007. 845
Dong, M. X., Li, F. L., Gao, D. Z., Geng, M. S., and Li, L. Y.: A study of the Late Miocene dry event based on sporo-pollen variations in Sunid Zuoqi, Inner Mongolia, Acta Geoscientica Sinica, 27, 207–212, 2006. 848
Dutton, J. F. and Barron, E. J.: Miocene to present vegetation changes: A possible piece of the Cenozoic cooling puzzle, Geology, 25, 39–41, 1997. 844
Eronen, J. T., Ataabadia, M. M., Micheelsb, A., Karme, A., Bernor, R. L., and Fortelius, M.: Distribution history and climatic controls of the Late Miocene Pikermian chronofauna, Proceedings of the National Academy of Sciences of the United States of America, 106, 11867–11871, 2009. 845, 847
Eronen, J. T., Puolamäki, K., Liu, L., Lintulaakso, K., Damuth, J., Janis, C., and Fortelius, M.: Precipitation and large herbivorous mammals , part II: Application to fossil data, Evol. Ecol. Res., 12, 235–248, 2010. 855, 884
Fluteau, F., Ramstein, G., and Besse, J.: Simulating the evolution of the Asian and African monsoons during the past 30 Myr using an atmospheric general circulation model, J. Geophys. Res.-Atmos., 104, 11995–12018, 1999. 843, 851, 858
Fortelius, M., Eronen, J., Jernvall, J., Liu, L. P., Pushkina, D., Rinne, J., Tesakov, A., Vislobokova, I., Zhang, Z. Q., and Zhou, L. P.: Fossil mammals resolve regional patterns of Eurasian climate change over 20 million years, Evolutionary Ecology Research, 4, 1005–1016, 2002. 855, 856
François, L., Ghislain, M., Otto, D., and Micheels, A.: Late Miocene vegetation reconstruction

CPD
7, 841–886, 2011

with the CARAIB model, Palaeogeogr. Palaeocl., 238, 302–320, 2006. 849
Gadgil, S.: The Indian monsoon and its variability, Annu. Rev. Earth Pl. Sc., 31, 429–467, 2003. 843, 853
Gao, X. J., Xu, Y., Zhao, Z. C., Pal, J. S., and Giorgi, F.: On the role of resolution and topography in the simulation of East Asia precipitation, Theor. Appl. Climatol., 86, 173–185, 2006. 844
Gao, X. J., Shi, Y., Song, R., Giorgi, F., Wang, Y., and Zhang, D.: Reduction of future monsoon precipitation over China: comparison between a high resolution RCM simulation and the driving GCM, Meteorol. Atmos. Phys., 100, 73–86, 2008. 844
Goswami, B. N. and Mohan, R. S. A.: Intraseasonal oscillations and interannual variability of the Indian summer monsoon, J. Climate, 14, 1180–1198, 2001. 853
Goswami, B. N., Krishnamurthy, V., and Annamalai, H.: A broad-scale circulation index for the interannual variability of the Indian summer monsoon, Q. J. Roy. Meteor. Soc., 125, 611–633, 1999. 875
Guo, Z. T., Ruddiman, W. F., Hao, Q. Z., Wu, H. B., Qiao, Y. S., Zhu, R. X., Peng, S. Z., Wei, J. J., Yuan, B. Y., and Liu, T. S.: Onset of Asian desertification by 22 Myr ago inferred from loess deposits in China, Nature, 416, 159–163, 2002. 843, 854, 883
Guo, Z. T., Sun, B., Zhang, Z. S., Peng, S. Z., Xiao, G. Q., Ge, J. Y., Hao, Q. Z., Qiao, Y. S., Liang, M. Y., Liu, J. F., Yin, Q. Z., and Wei, J. J.: A major reorganization of Asian climate by the early Miocene, Clim. Past, 4, 153–174, doi:10.5194/cp-4-153-2008, 2008. 856
Harris, N.: The elevation history of the Tibetan Plateau and its implications for the Asian monsoon, Palaeogeogr. Palaeocl., 241, 4–15, 2006. 844
Harzhauser, M. and Piller, W. E.: Benchmark data of a changing sea - Palaeogeography, palaeobiogeography and events in the Central Paratethys during the Miocene, Palaeogeogr. Palaeocl., 253, 8–31, 2007. 846
Hollweg, H. D., Bohm, U., Fast, I., Hennemuth, B., Keuler, K., Keup-Thiel, E., Lautenschlager, M., and Legutke, S.: Ensemble simulations over Europe with the regional climate model CLM forced with IPCC AR4 global scenarios, Tech. Rep. 3, M&D, Max Planck Institute for Meteorology, 2008. 845
Hoorn, C., Ohja, T., and Quade, J.: Palynological evidence for vegetation development and climatic change in the Sub-Himalayan Zone (Neogene, Central Nepal), Palaeogeogr. Palaeocl., 163, 133–161, 2000. 849, 857, 883
Huang, Y. S., Clemens, S. C., Liu, W. G., Wang, Y., and Prell, W. L.: Large-scale hydrological change drove the late Miocene C_4 plant expansion in the Himalayan foreland and Arabian

CPD
7, 841–886, 2011

Peninsula, Geology, 35, 531–534, 2007. 843, 856, 883
Jacques, F. M. B., Guo, S. X., Su, T., Xing, Y. W., Huang, Y. J., Liu, Y. S., Ferguson, D. K., and Zhou, Z. K.: Quantitative reconstruction of the Late Miocene monsoon climates of southwest China: A case study of the Lincang flora from Yunnan Province, Palaeogeogr. Palaeocl., doi:10.1016/j.palaeo.2010.04.014, in press, 2010. 857
Jaeger, E. B., Anders, I., Luthi, D., Rockel, B., Schar, C., and Seneviratne, S. I.: Analysis of ERA40-driven CLM simulations for Europe, Meteorologische Zeitschrift, 17, 349–367, 2008. 845
Jia, G. D., Peng, P. A., Zhao, Q. H., and Jian, Z. M.: Changes in terrestrial ecosystem since 30 Ma in East Asia: Stable isotope evidence from black carbon in the South China Sea, Geology, 31, 1093–1096, 2003. 854, 855, 883
Jiang, H. and Ding, Z.: Spatial and temporal characteristics of Neogene palynoflora in China and its implication for the spread of steppe vegetation, J. Arid Environ., 73, 765–772, 2009. 855
Jiang, H. C. and Ding, Z. L.: A 20 Ma pollen record of East-Asian summer monsoon evolution from Guyuan, Ningxia, China, Palaeogeogr. Palaeocl., 265, 30–38, 2008. 843, 855, 860, 883
Ju, L. X., Wang, H. K., and Jiang, D. B.: Simulation of the Last Glacial Maximum climate over East Asia with a regional climate model nested in a general circulation model, Palaeogeogr. Palaeocl., 248, 376–390, 2007. 844
Kaakinen, A., Sonninen, E., and Lunkka, J. P.: Stable isotope record in paleosol carbonates from the Chinese Loess Plateau: Implications for late Neogene paleoclimate and paleovegetation, Palaeogeogr. Palaeocl., 237, 359–369, 2006. 856
Kottek, M., Grieser, J., Beck, C., Rudolf, B., and Rubel, F.: World map of the Köppen-Geiger climate classification updated, Meteorologische Zeitschrift, 15, 259–263, 2006. 852
Kroon, D., Steens, T., and Troelstra, S. R.: Onset of monsoonal related upwelling in the western Arabian Sea as revealed by planktonic foraminifers, Proceedings of the Ocean Drilling Program, 117, 257–263, 1991. 843, 856
Kutzbach, J. E., Prell, W. L., and Ruddiman, W. F.: Sensitivity of Eurasian Climate to Surface Uplift of the Tibetan Plateau, J. Geol., 101, 177–190, 1993. 843
Lacombe, O., Mouthereau, F., Kargar, S., and Meyer, B.: Late Cenozoic and modern stress fields in the western Fars (Iran): Implications for the tectonic and kinematic evolution of central Zagros, Tectonics, 25, TC1003, doi:10.1029/2005TC001831, 2006. 848

CPD
7, 841–886, 2011

Li, J. G. and Zhang, Y. Y.: Neogene palynofloras from east offshore, Hainan Island, Acta Palaeontologica Sinica, 15, 323–330, 1998. 849
Liu, G. W.: Late Cenozoic palynological sequence of Eastern Qinghai-Xizang Plateau and its bearing on palaeogeography, Acta Micropalaeontologica Sinica, 13, 363–372, 1996. 848
Liu, G. W.: A Miocene palynoflora from Huanan County of Heilongjiang Province, Northeastern China, Acta Micropalaeontologica Sinica, 15, 48–54, 1998. 849
Liu, J., Wang, B., and Yang, J.: Forced and internal modes of variability of the East Asian summer monsoon, Clim. Past, 4, 225–233, doi:10.5194/cp-4-225-2008, 2008. 852
Liu, L. P., Eronen, J. T., and Fortelius, M.: Significant mid-latitude aridity in the middle Miocene of East Asia, Palaeogeogr. Palaeocl., 279, 201–206, 2009. 855
Liu, X. D. and Yin, Z. Y.: Sensitivity of East Asian monsoon climate to the uplift of the Tibetan Plateau, Palaeogeogr. Palaeocl., 183, 223–245, 2002. 843
Liu, Y.-S., Utescher, T., Zhou, Z., and Sun, B.: The evolution of Miocene climates in North China: Preliminary results of quantitative reconstructions from plant fossil records, Palaeogeogr. Palaeocl., doi:10.1016/j.palaeo.2010.07.004, in press, 2010. 855
Liu-Zeng, J., Tapponnier, P., Gaudemer, Y., and Ding, L.: Quantifying landscape differences across the Tibetan plateau: Implications for topographic relief evolution, J. Geophys. Res.-Earth Surface, 113, F04018, doi:10.1029/2007jf000897, 2008. 848
Lunt, D. J., Flecker, R., Valdes, P. J., Salzmann, U., Gladstone, R., and Haywood, A. M.: A methodology for targeting palaeo proxy data acquisition: A case study for the terrestrial late Miocene, Earth Planet. Sci. Lett., 271, 53–62, 2008. 844
Ma, Y. Z., Li, J. J., and Fang, X. M.: Pollen assemblage in 30.6-5.0 Ma redbeds of Linxia region and climate evolution, Chinese Science Bulletin, 43, 301–304, 1998. 848, 858
Ma, Y. Z., Fang, X. M., Li, J. J., Wu, F. L., and Zhang, J.: The vegetation and climate change during Neocene and Early Quaternary in Jiuxi Basin, China, Science in China Series D-Earth Sciences, 48, 676–688, 2005. 858
Micheels, A., Bruch, A. A., Uhl, D., Utescher, T., and Mosbrugger, V.: A Late Miocene climate model simulation with ECHAM4/ML and its quantitative validation with terrestrial proxy data, Palaeogeogr. Palaeocl., 253, 251–270, 2007. 844, 846, 849
Micheels, A., Bruch, A., and Mosbrugger, V.: Miocene climate modelling sensitivity experiments for different CO_2 concentrations, Palaeontologia Electronica, 12, 5A, 20 p., 2009a. 846
Micheels, A., Eronen, J., and Mosbrugger, V.: The Late Miocene climate response to a modern Sahara desert, Global Planet. Change, 67, 193–204, 2009b. 859

CPD
7, 841–886, 2011

Micheels, A., Bruch, A. A., Eronen, J., Fortelius, M., Harzhauser, M., Utescher, T., and Mosbrugger, V.: Analysis of heat transport mechanisms from a Late Miocene model experiment with a fully-coupled atmosphere-ocean general circulation model, Palaeogeogr. Palaeocl., doi:10.1016/j.palaeo.2010.09.021, in press, 2010. 844, 845, 847, 859

Mitchell, T. D. and Jones, P. D.: An improved method of constructing a database of monthly climate observations and associated high-resolution grids, Int. J. Climatol., 25, 693–712, 2005. 881

Molnar, P., Boos, W. R., and Battisti, D. S.: Orographic controls on climate and paleoclimate of Asia: Thermal and mechanical roles for the Tibetan Plateau, Annu. Rev. Earth Pl. Sc., 38, 77–102, 2010. 843

Park, S. and Hong, S. Y.: The role of surface boundary forcing over south Asia in the Indian summer monsoon circulation: A regional climate model sensitivity study, Geophys. Res. Lett., 31, L12112, doi:10.1029/2004GL019729, 2004. 844

Passey, B. H., Ayliffe, L. K., Kaakinen, A., Zhang, Z. Q., Eronen, J. T., Zhu, Y. M., Zhou, L. P., Cerling, T. E., and Fortelius, M.: Strengthened East Asian summer monsoons during a period of high-latitude warmth? Isotopic evidence from Mio-Pliocene fossil mammals and soil carbonates from northern China, Earth Planet. Sci. Lett., 277, 443–452, 2009. 843, 844, 855, 856, 860, 883

Pearson, P. N. and Palmer, M. R.: Atmospheric carbon dioxide concentrations over the past 60 million years, Nature, 406, 695–699, 2000. 846

Pettke, T., Halliday, A. N., Hall, C. M., and Rea, D. K.: Dust production and deposition in Asia and the north Pacific Ocean over the past 12 Myr, Earth Planet. Sci. Lett., 178, 397–413, 2000. 858

Popov, S. V., Rögl, F., Rozanov, A. Y., Steininger, F., Shcherba, I., and Kovac, M.: Lithological-Paleogeographic maps of Paratethys: 10 Maps Late Eocene to Pliocene, Courier Forschungsinstitut Senckenberg, 250, 1–46, 2004. 846

Qiang, X. K., Li, Z. X., Powell, C. M., and Zheng, H. B.: Magnetostratigraphic record of the Late Miocene onset of the East Asian monsoon, and Pliocene uplift of northern Tibet, Earth Planet. Sci. Lett., 187, 83–93, 2001. 854

Quade, J., Cerling, T. E., and Bowman, J. R.: Development of Asian monsoon revealed by marked ecological shift during the Latest Miocene in Northern Pakistan, Nature, 342, 163–166, 1989. 843, 857, 883

Ramstein, G., Fluteau, F., Besse, J., and Joussaume, S.: Effect of orogeny, plate motion and

CPD
7, 841–886, 2011

land sea distribution on Eurasian climate change over the past 30 million years, Nature, 386, 788–795, 1997. 843, 858
Raschendorfer, M.: The new turbulence parameterization of LM, COSMO newsletter, 1, 90–98, 2001. 845
Rea, D. K., Snoeckx, H., and Joseph, L. H.: Late Cenozoic eolian deposition in the North Pacific: Asian drying, Tibetan uplift, and cooling of the northern hemisphere, Paleoceanography, 13, 215–224, 1998. 843, 854, 883
Rockel, B. and Geyer, B.: The performance of the regional climate model CLM in different climate regions, based on the example of precipitation, Meteorologische Zeitschrift, 17, 487–498, 2008. 845
Rowley, D. B. and Currie, B. S.: Palaeo-altimetry of the late Eocene to Miocene Lunpola basin, central Tibet, Nature, 439, 677–681, 2006. 848
Rowley, D. B., Pierrehumbert, R. T., and Currie, B. S.: A new approach to stable isotope-based paleoaltimetry: implications for paleoaltimetry and paleohypsometry of the High Himalaya since the Late Miocene, Earth Planet. Sci. Lett., 188, 253–268, 2001. 848
Ruddiman, W. F. and Kutzbach, J. E.: Forcing of late Cenozoic Northern Hemisphere climate by plateau uplift in Southern Asia and the American West, J. Geophys. Res.-Atmos., 94, 18409–18427, 1989. 843
Sakai, K. and Kawamura, R.: Remote response of the East Asian winter monsoon to tropical forcing related to El Niño-Southern Oscillation, J. Geophys. Res.-Atmos., 114, D06105, doi:10.1029/2008JD010824, 2009. 875
Sanyal, P., Sarkar, A., Bhattacharya, S. K., Kumar, R., Ghosh, S. K., and Agrawal, S.: Intensification of monsoon, microclimate and asynchronous C_4 appearance: Isotopic evidence from the Indian Siwalik sediments, Palaeogeogr. Palaeocl., 296, 165–173, 2010. 844, 857
Schrodin, R. and Heise, E.: A new multi-layer soil model, COSMO Newsletter, 2, 149–151, 2002. 845
Shu, J. W., Wang, W. M., Leopold, E. B., Wang, J. S., and Yin, D. S.: Pollen stratigraphy of coal-bearing deposits in the Neogene Jidong Basin, Heilongjiang Province, NE China: New insights on palaeoenvironment and age, Rev. Palaeobot. Palyno., 148, 163–183, 2008. 849
Singh, G. P. and Oh, J. H.: Impact of Indian Ocean sea-surface temperature anomaly on Indian summer monsoon precipitation using a regional climate model, Int. J. Climatol., 27, 1455–1465, 2007. 843, 844
Skamarock, W. C. and Klemp, J. B.: The stability of time-split numerical-methods for the hydro-

CPD
7, 841–886, 2011

static and the nonhydrostatic elastic equations, Mon. Weather Rev., 120, 2109–2127, 1992. 845
Smiatek, G., Rockel, B., and Schattler, U.: Time invariant data preprocessor for the climate version of the COSMO model (COSMO-CLM), Meteorologische Zeitschrift, 17, 395–405, 2008. 848
Spicer, R. A., Harris, N. B. W., Widdowson, M., Herman, A. B., Guo, S. X., Valdes, P. J., Wolfe, J. A., and Kelley, S. P.: Constant elevation of southern Tibet over the past 15 million years, Nature, 421, 622–624, 2003. 848
Steinke, S., Groeneveld, J., Johnstone, H., and Rendle-Buhring, R.: East Asian summer monsoon weakening after 7.5 Ma: Evidence from combined planktonic foraminifera Ma/Ca and $\delta^{18}O$ (ODP site 1146; northern South China Sea), Palaeogeogr. Palaeocl., 289, 33–43, 2010. 856
Steppuhn, A., Micheels, A., Geiger, G., and Mosbrugger, V.: Reconstructing the Late Miocene climate and oceanic heat flux using the AGCM ECHAM4 coupled to a mixed-layer ocean model with adjusted flux correction, Palaeogeogr. Palaeocl., 238, 399–423, 2006. 844, 846
Steppuhn, A., Micheels, A., Bruch, A. A., Uhl, D., Utescher, T., and Mosbrugger, V.: The sensitivity of ECHAM4/ML to a double CO_2 scenario for the Late Miocene and the comparison to terrestrial proxy data, Global Planet. Change, 57, 189–212, 2007. 844, 846
Sun, D. H.: Monsoon and westerly circulation changes recorded in the late Cenozoic aeolian sequences of Northern China, Global Planet. Change, 41, 63–80, 2004. 854
Sun, D. H., Shaw, J., An, Z. S., Cheng, M. Y., and Yue, L. P.: Magnetostratigraphy and paleoclimatic interpretation of a continuous 7.2Ma Late Cenozoic eolian sediments from the Chinese Loess Plateau, Geophys. Res. Lett., 25, 85–88, 1998. 854
Sun, J. M. and Zhang, Z. Q.: Palynological evidence for the Mid-Miocene Climatic Optimum recorded in Cenozoic sediments of the Tian Shan Range, northwestern China, Global and Planetary Change, 64, 53–68, 2008. 848, 857
Sun, J. M., Zhang, Z. Q., and Zhang, L. Y.: New evidence on the age of the Taklimakan Desert, Geology, 37, 159–162, 2009. 848, 858
Sun, X. J. and Wang, P. X.: How old is the Asian monsoon system? Palaeobotanical records from China, Palaeogeogr. Palaeocl., 222, 181–222, 2005. 843, 856
Tang, L. Y. and Shen, C. M.: Late Cenozoic vegetational history and climatic characteristics of Qinghai-Xizang Plateau, Acta Micropalaeontologica Sinica, 13, 321–337, 1996. 848
Tapponnier, P., Xu, Z. Q., Roger, F., Meyer, B., Arnaud, N., Wittlinger, G., and Yang, J. S.:

CPD
7, 841–886, 2011

Oblique stepwise rise and growth of the Tibet plateau, Science, 294, 1671–1677, 2001. 848
Tiedtke, M.: A comprehensive mass flux scheme for cumulus parameterization in large-scale models, Mon. Weather Rev., 117, 1779–1800, 1989. 845
Wan, S. M., Li, A. C., Clift, P. D., and Stuut, J. B. W.: Development of the East Asian monsoon: Mineralogical and sedimentologic records in the northern South China Sea since 20 Ma, Palaeogeogr. Palaeocl., 254, 561–582, 2007. 854
Wang, B., Wu, Z. W., Li, J. P., Liu, J., Chang, C. P., Ding, Y. H., and Wu, G. X.: How to measure the strength of the East Asian summer monsoon, J. Climate, 21, 4449–4463, 2008a. 843, 856, 875
Wang, H. J. and Jiang, D. B.: A new East Asian winter monsoon intensity index and atmospheric circulation comparison between strong and weak composite, Quaternary Sciences, 24, 19–27, 2004. 875
Wang, J., Wang, Y. J., Liu, Z. C., Li, J. Q., and Xi, P.: Cenozoic environmental evolution of the Qaidam Basin and its implications for the uplift of the Tibetan Plateau and the drying of central Asia, Palaeogeogr. Palaeocl., 152, 37–47, 1999. 848
Wang, P. X., Clemens, S., Beaufort, L., Braconnot, P., Ganssen, G., Jian, Z. M., Kershaw, P., and Sarnthein, M.: Evolution and variability of the Asian monsoon system: state of the art and outstanding issues, Quaternary Sci. Rev., 24, 595–629, 2005. 843
Wang, W. M., Saito, T., and Nakagawa, T.: Palynostratigraphy and climatic implications of Neogene deposits in the Himi area of Toyama Prefecture, Central Japan, Rev. Palaeobot. Palyno., 117, 281–295, 2001. 849
Wang, Y., Wang, X. M., Xu, Y. F., Zhang, C. F., Li, Q., Tseng, Z. J., Takeuchi, G., and Deng, T.: Stable isotopes in fossil mammals, fish and shells from Kunlun Pass Basin, Tibetan Plateau: Paleo-climatic and paleo-elevation implications, Earth Planet. Sci. Lett., 270, 73–85, 2008b. 848
Webster, P. J., Magana, V. O., Palmer, T. N., Shukla, J., Tomas, R. A., Yanai, M., and Yasunari, T.: Monsoons: Processes, predictability, and the prospects for prediction, J. Geophys. Res.-Oceans, 103, 14 451–14 510, 1998. 875
Wolfe, J. A.: Distribution of major vegetation types during the Tertiary, in: The carbon cycle and atmospheric CO_2: Natural Variations Archean to Present, edited by Sundquist, E. T. and Broecker, W. S., 357–375, AGU, Washington, DC, 1985. 848
Xia, K., Su, T., Liu, Y. S., Xing, Y. W., Jacques, F. M. B., and Zhou, Z. K.: Quantitative climate reconstructions of the late Miocene Xiaolongtan megaflora from Yunnan, southwest China,

CPD
7, 841–886, 2011

Palaeogeogr. Palaeocl., 276, 80–86, 2009. 849, 857
Yue, X., Wang, H. J., Wang, Z. F., and Fan, K.: Simulation of dust aerosol radiative feedback using the Global Transport Model of Dust: 1. Dust cycle and validation, J. Geophys. Res.-Atmos., 114, D10202, doi:10.1029/2008JD010995, 2009. 855
Zachos, J., Pagani, M., Sloan, L., Thomas, E., and Billups, K.: Trends, rhythms, and aberrations in global climate 65 Ma to present, Science, 292, 686–693, 2001. 843
Zhang, Z. S., Wang, H. J., Guo, Z. T., and Jiang, D. B.: Impacts of tectonic changes on the reorganization of the Cenozoic paleoclimatic patterns in China, Earth Planet. Sci. Lett., 257, 622–634, 2007a. 860
Zhang, Z. S., Wang, H. J., Guo, Z. T., and Jiang, D. B.: What triggers the transition of palaeoenvironmental patterns in China, the Tibetan Plateau uplift or the Paratethys Sea retreat?, Palaeogeogr. Palaeocl., 245, 317–331, 2007b. 860
Zheng, D. W., Zhang, P. Z., Wan, J. L., Yuan, D. Y., Li, C. Y., Yin, G. M., Zhang, G. L., Wang, Z. C., Min, W., and Chen, J.: Rapid exhumation at similar to 8 Ma on the Liupan Shan thrust fault from apatite fission-track thermochronology: Implications for growth of the northeastern Tibetan Plateau margin, Earth Planet. Sci. Lett., 248, 198–208, 2006. 848
Zheng, H. B., Powell, C. M., An, Z. S., Zhou, J., and Dong, G. R.: Pliocene uplift of the northern Tibetan Plateau, Geology, 28, 715–718, 2000. 848
Zheng, Y. H. and Wang, W. X.: Sequence of Miocene Fotan Group in SE Fujian and its palynoassemblages, Acta Palaeontologica Sinica, 33, 200–218, 1994. 849
Zheng, Y. Q., Yu, G., Wang, S. M., Xue, B., Zhuo, D. Q., Zeng, X. M., and Liu, H. Q.: Simulation of paleoclimate over East Asia at 6 ka BP and 21 ka BP by a regional climate model, Clim. Dynam., 23, 513–529, 2004. 844
Zhu, J. H. and Wang, S. W.: 80 yr oscillation of summer rainfall over North China and East Asian Summer Monsoon, Geophys. Res. Lett., 29, 1672, doi:10.1029/2001GL013997, 2002. 843
Zhu, Y. M., Zhou, L. P., Mo, D. W., Kaakinen, A., Zhang, Z. Q., and Fortelius, M.: A new magnetostratigraphic framework for late Neogene Hipparion Red Clay in the eastern Loess Plateau of China, Palaeogeogr. Palaeocl., 268, 47–57, 2008. 854

CPD
7, 841–886, 2011

Table 1. The setup of the Tortonian physical boundary conditions in the global model (GTORT) and the regional model (TORT). For GTORT, the boundary configurations within the regional model domain are in bold.

Boundary conditions	GTORT	TORT
Orography	Tibetan Plateau (TP): 70% of (present-day height); lower Greenland, Alps and other orography	northern TP: 30% (of present-day height); central and southeastern TP: 80%; southern TP: 100%; Tian Shan, Gobi Altai and Zagros: 70%; other orography: 70–90%
Vegetation	northward expansion of warm forest in E-Asia; grassland to savanna over C-Asia, W-Asia and Sahara; boreal forest over the northern high latitudes including Greenland	northward expansion of temperate deciduous forest in E-Asia; grassland over C-Asia; mixed-leaf forest in the southern TP; open forest in the northern TP and the Loess Plateau
Land-sea distribution	presence of the Paratethys and the Pannonian Lake; open Panama Isthmus with a depth of 500 m; southward shift of Australia	presence of the Paratethys with the same extent as GTORT
pCO_2	same as GCTRL (360 ppm)	same as CTRL (360 ppm)
Orbital parameters	present-day	present-day

CPD
7, 841–886, 2011

Table 2. Summary of the regional model experiments.

Experiments	CTRL	TORT	TORTPD	PDTORT
Initial and lateral boundary forcings	GCTRL	GTORT	GTORT	GCTRL
Physical boundary conditions	present-day	Tortonian	present-day	Tortonian

CPD
7, 841–886, 2011

Table 3. The comparison of annual precipitation (mm day^{-1}), winter and summer monsoon indices between the global and regional model experiments. E-China: 105–120° E, 22–42° N; India: 70–100° E,10–30° N; MO: DJF sea-level pressure difference between the Siberian High (106.1° E, 52.9° N) and the Aleutian Low (145.0° E, 43.6° N) (based on Sakai and Kawamura, 2009); WJ: DJF 850 hPa wind speed over E-Asia (115–130° E, 25–50° N) (based on Wang and Jiang, 2004); EIMR: JJAS precipitation over the extended Indian region (70–110° E, 10–30° N) (based on Goswami et al., 1999); WY: JJA zonal wind difference between the lower troposphere at 850 hPa and the upper troposphere at 200 hPa over S-Asia (60–110° E, 5–20° N) (based on Webster et al., 1998); WN: JJA meridional wind velocity at 850 hPa over E-China (110-125° E, 20–40° N) (based on Wang et al., 2008a); WYF: JJA meridional wind difference between S-China (110–125° E, 20–30° N) and N-China (110–125° E, 30–40° N) (based on Wang et al., 2008a).

	GCTRL	GTORT	GTORT-GCTRL	CTRL	TORT	TORT-CTRL	TORTPD-CTRL	PDTORT-CTRL
Annual Precipitation								
Domain	2.97	3.21	0.23	1.98	2.14	0.16	0.20	0.01
Land	2.13	2.16	0.03	1.53	1.56	0.03	0.09	−0.01
Sea	4.58	5.19	0.62	2.84	3.24	0.40	0.42	0.05
E-China	4.37	2.97	−1.40	2.02	1.58	−0.44	−0.12	−0.29
India	3.70	4.34	0.64	2.18	2.25	0.07	0.25	−0.07
Winter monsoon indices								
MO	25.58	20.84	−4.74	19.57	14.25	−5.32	−4.25	−0.57
WJ	8.74	9.95	1.21	9.47	10.51	1.04	0.67	0.49
Summer monsoon indices								
EIMR	858.53	1031.53	172.99	552.62	628.88	76.25	121.30	−13.74
WY	26.20	24.07	−2.12	25.92	23.19	−2.73	−1.85	−0.34
WN	1.86	1.98	0.12	1.58	1.01	−0.56	−0.03	−0.43
WYF	0.40	1.21	0.82	0.27	0.84	0.57	0.67	0.18

CPD
7, 841–886, 2011

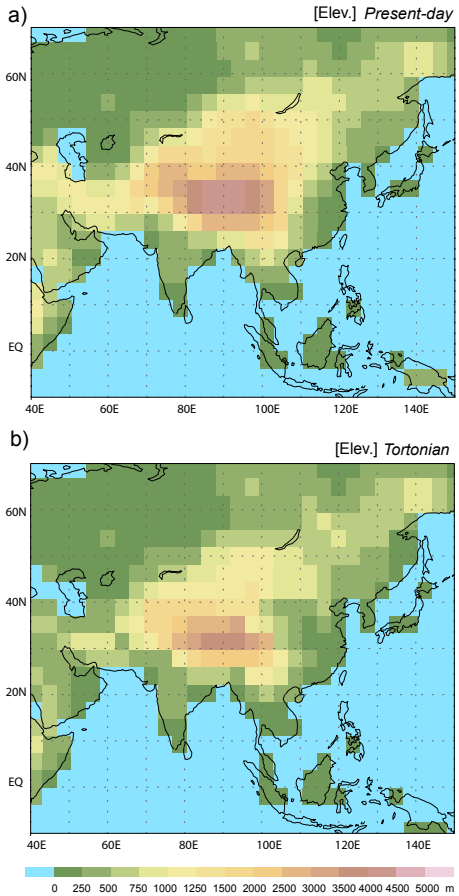

Fig. 1. The orography of the present-day control run **(a)** and the Tortonian run **(b)** in the global model.

CPD
7, 841–886, 2011

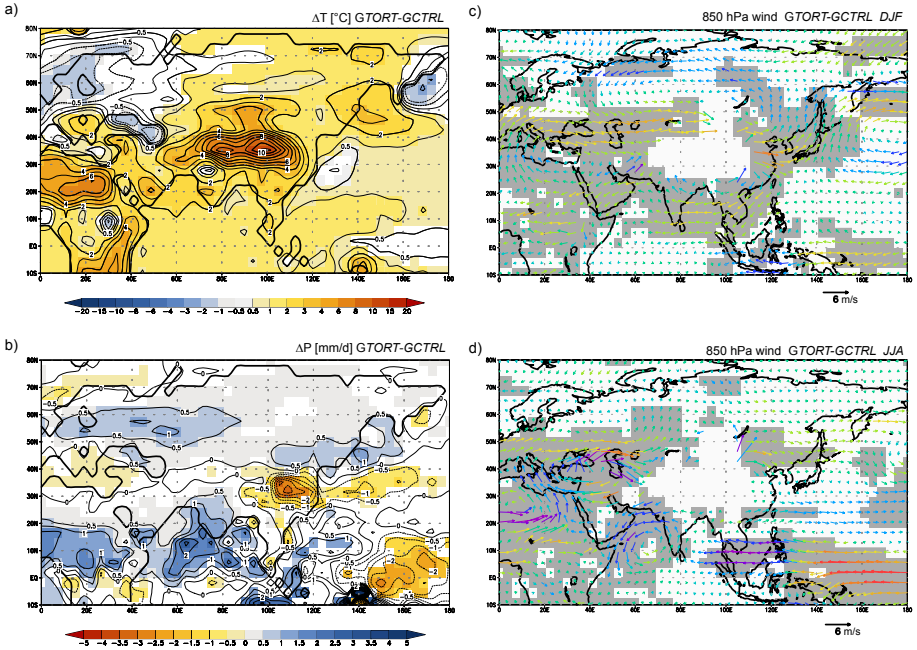

Fig. 2. The annual average difference for temperature (°C) **(a)** and precipitation (mm d^{-1}) **(b)**, and the wind anomalies at 850 hPa for winter (DJF) **(c)** and summer (JJA) **(d)** between the Tortonian (GTORT) and the present-day control (GCTRL) run of the global model. The coloured or shaded areas have the significant anomalies with a Student's t-test ($p = 0.05$). The colour of vectors denotes the changes in wind speed (yellow red = increase, blue purple = decrease).

CPD
7, 841–886, 2011

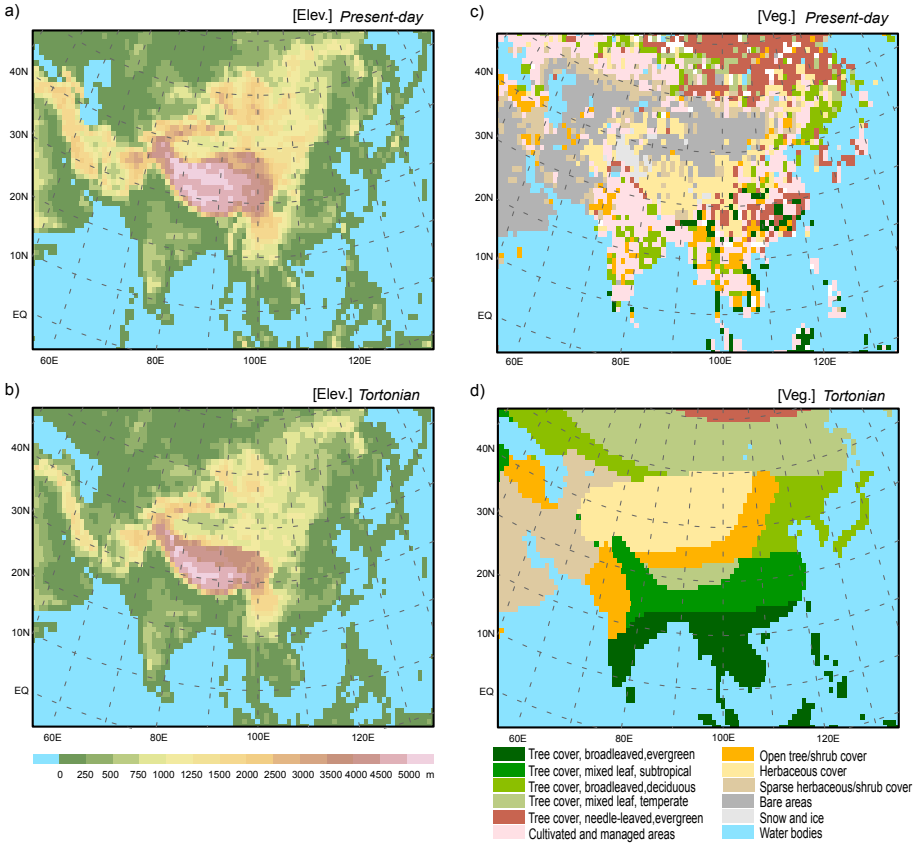

Fig. 3. The orography and vegetation for the present-day control run **(a, c)** and the Tortonian run **(b, d)** in the regional model. The present-day vegetation is based on the GLC2000 data set which is used in the regional model by default.

CPD
7, 841–886, 2011

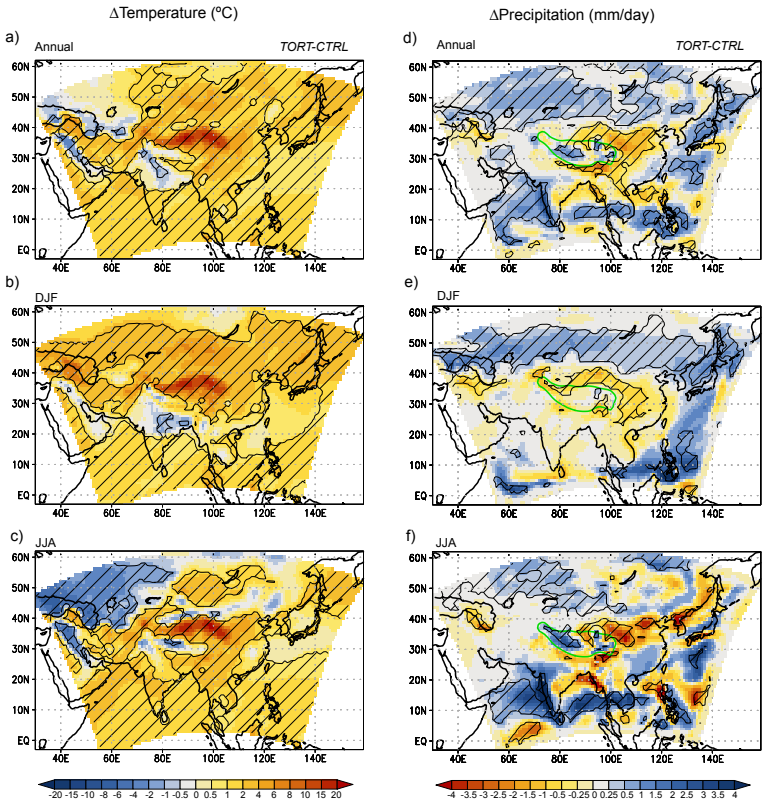

Fig. 4. Temperature (°C) and precipitation (mm day^{-1}) difference between TORT and CTRL. **(a, d)** Annual, **(b, e)** winter (DJF), **(c, f)** summer (JJA). The hatched areas have the significant anomalies with a Student's t-test ($p = 0.05$). The green contour denotes the extent of the Tibetan Plateau (>3000 m) in TORT. Note that the sponge layer (the outermost 8 grid cells) of the regional model domain is kept in the figures.

CPD
7, 841–886, 2011

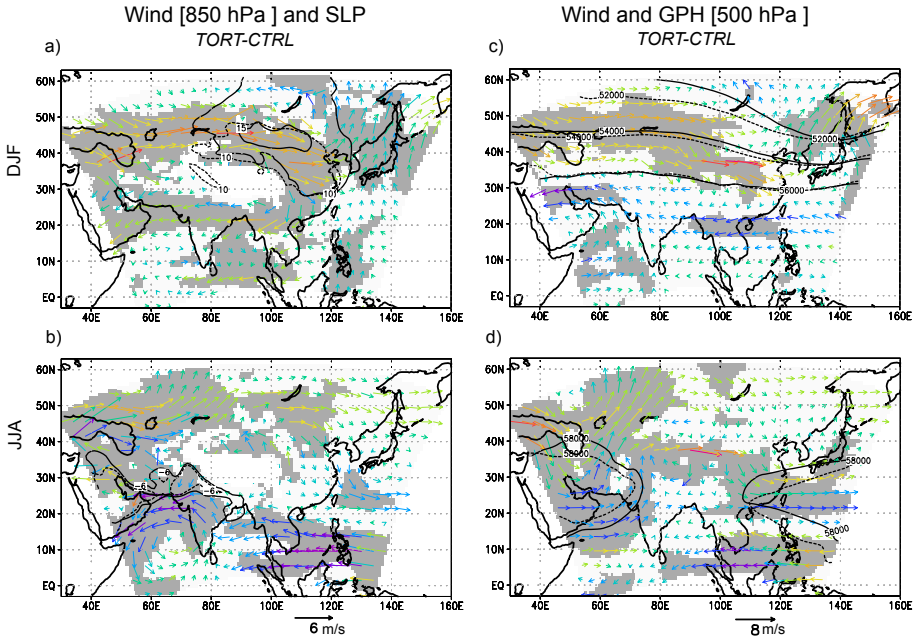

Fig. 5. Winter (DJF) and summer (JJA) wind anomalies (m s^{-1}) at 850 hPa **(a, b)** and 500 hPa **(c, d)** between TORT and CTRL. The grey shaded areas indicate the regions where either the zonal or the meridional wind anomalies are significant with a Student's t-test ($p = 0.05$). The contour lines represent the sea level pressure (SLP) (hPa) or the geopotential height (m^2 s^{-2}) anomalies to the domain average in CTRL (solid) and TORT (dashed). The colour of vectors denotes the changes in wind speed (yellow red = increase, blue purple = decrease).

CPD
7, 841–886, 2011

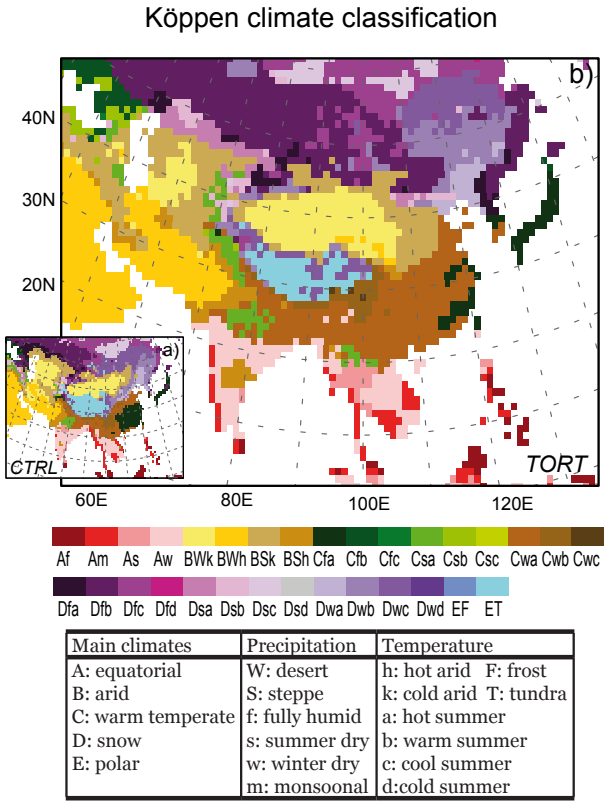

Fig. 6. The Köppen-Geiger climate classification. **(a)** the present-day (CTRL), **(b)** the Tortonian (TORT) based on the regional model result. For the present-day classification, the temperature fields are derived from CRU TS 2.1 data set (Mitchell and Jones, 2005). The precipitation fields are derived from GPCC VASClimOv1.1 data set (Beck et al., 2005). To generate a similar data set for the Tortonian classification, we add the anomalies of the temperature and precipitation between TORT and CTRL to the present-day observation data set.

CPD
7, 841–886, 2011

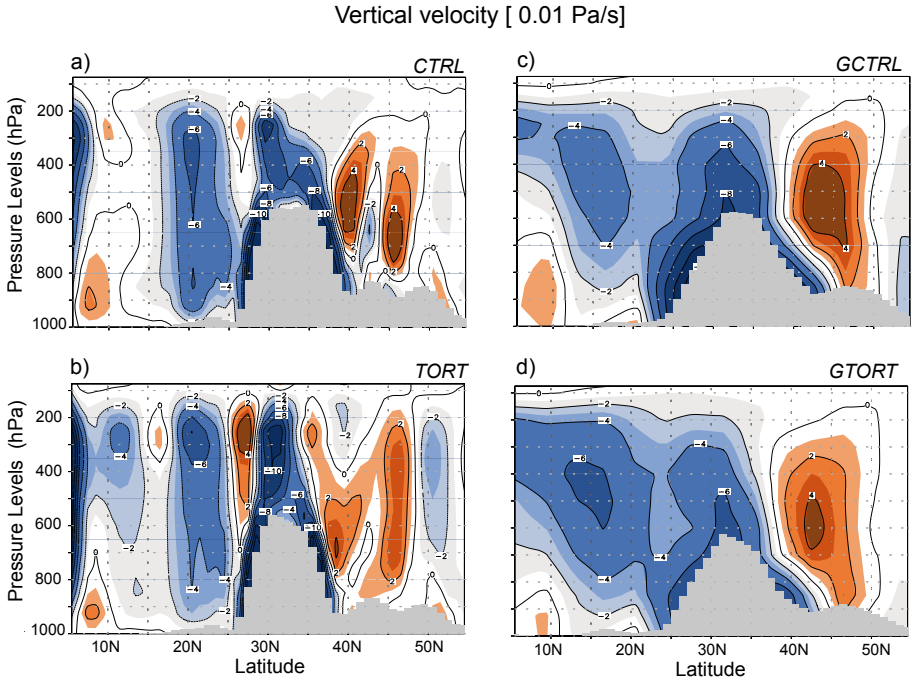

Fig. 7. Zonal averaged vertical wind velocity (10^{-2}Pa s^{-1}) over longitude between 80° E and 95° E in the summer season (JJA). **(a)** CTRL, **(b)** TORT, **(c)** GCTRL, **(d)** GTORT. The blue colour denotes upward motion and the red colour denotes sinking motion. The grid cells with pressure larger than the surface pressure are shaded by gray colour.

CPD
7, 841–886, 2011

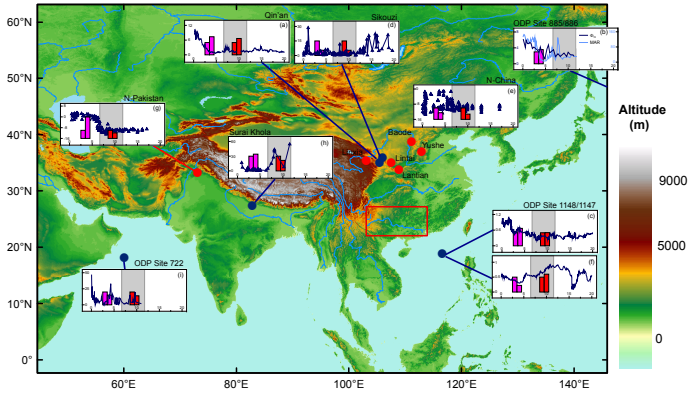

Fig. 8. Proxy records of the Asian monsoon variation in the Neogene and the comparison with the global model (purple bars – left: GCTRL; right: GTORT) and regional model (red bars – left: CTRL; right: TORT) results. **(a)** dust accumulation rate (cm kyr^{-1}), Loess Plateau, N-China (Guo et al., 2002); compared with the 500 hPa wind speed (DJF) in the model. **(b)** Mass accumulation rate (right axis, mg cm^{-2} kyr^{-1}) and grain size (left axis, ϕ_{50}), ODP site 885/886 (Rea et al., 1998); compared with the 500 hPa wind speed (DJF). **(c)** Black carbon accumulation rate (mg cm^{-2} kyr^{-1})), ODP site 1147/1148 (Jia et al., 2003); compared with the 850 hPa wind speed (DJF); **(d)** Humidity index, Sikouzi, N-China (Jiang and Ding, 2008); compared with the mean annual precipitation; **(e)** δ^{13}C (‰, VPBD) of tooth enamel, localities denoted by red dots, N-China (Passey et al., 2009); compared with the mean JJA-precipitation; **(f)** Chemical weathering index (C_{RAT}), ODP site 1148 (Clift et al., 2008); compared with the mean annual runoff over the reach of Pearl river as denoted by the red rectangular; **(g)** δ^{13}C (‰, PBD) of pedogenic carbonate, Northern Pakistan (Quade et al., 1989); compared with the mean JJA-precipitation; **(h)** *Quercus* (%), Central Nepal (Hoorn et al., 2000); compared with the mean annual precipitation; **(i)** *G. Bulloides* (%), ODP site 722 (Huang et al., 2007); compared with the 850 hPa wind speed (JJA). In all cases, the x-axis represents the age (Ma). The light gray shaded area denotes the Tortonian (11–7 Ma). All the bars are shown in relative scale.

CPD
7, 841–886, 2011

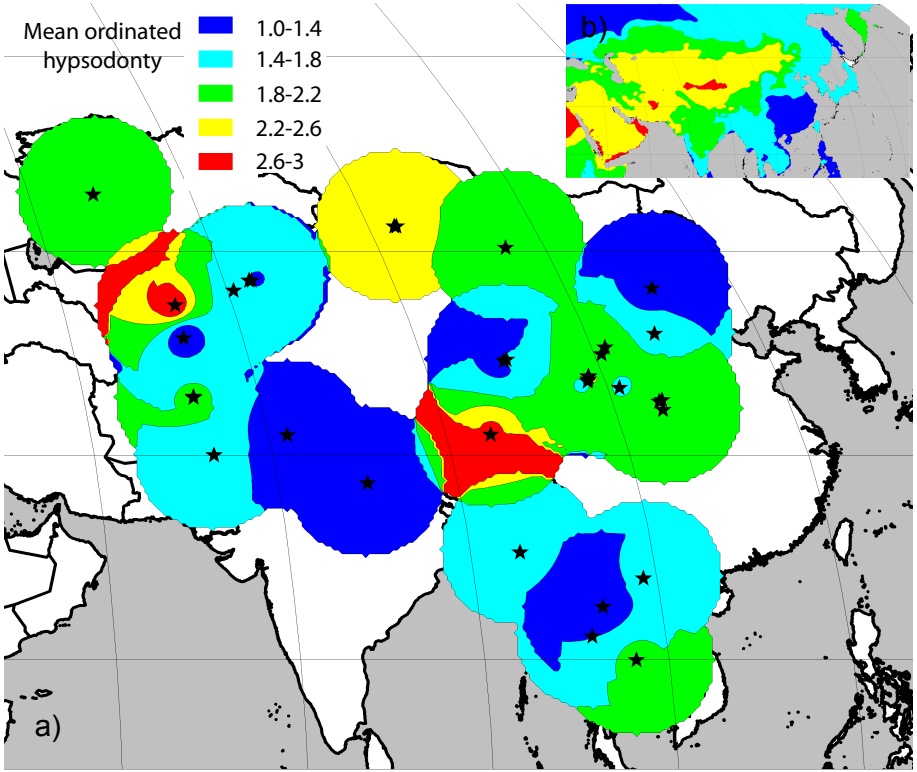

Fig. 9. The colour-interpolated map of large mammal plant-eater mean hypsodonty by locality in Asia during the early Late Miocene (11–8 Ma) **(a)** compared with the present day **(b)** (Eronen et al., 2010). The higher hypsodonty represents lower precipitation and vice versa.

CPD
7, 841–886, 2011

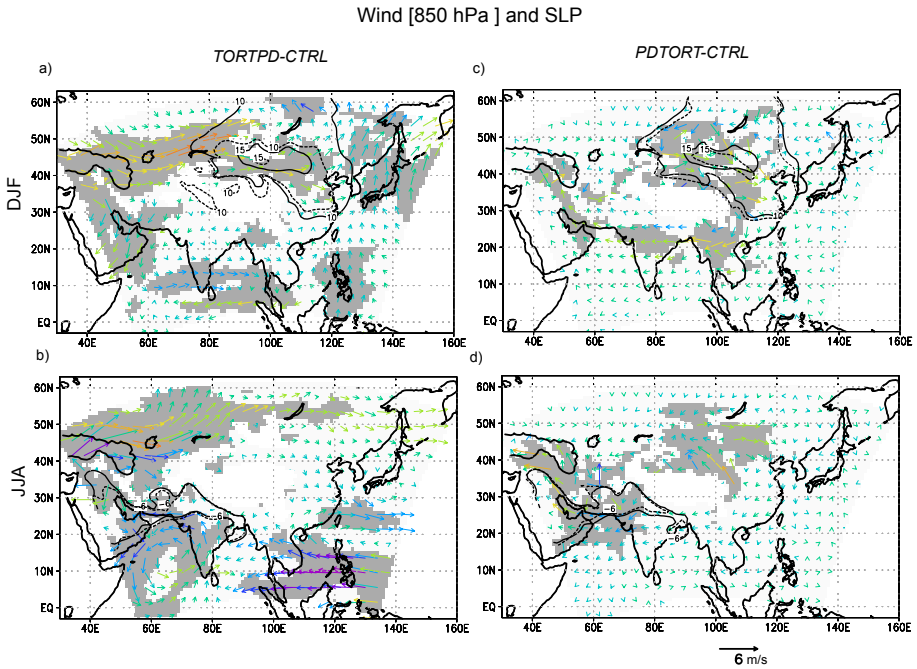

Fig. 10. 850 hPa wind anomalies ($m\,s^{-1}$) of TORTPD and PDTORT runs to the present-day control run (CTRL). **(a)** TORTPD minus CTRL, DJF; **(b)** TORTPD minus CTRL, JJA; **(c)** PDTORT minus CTRL, DJF; **(d)** PDTORT minus CTRL, JJA. The grey shaded areas indicate the regions where either the zonal or the meridional wind anomalies are significant with a Student's t-test ($p = 0.05$). The contour lines represent the sea level pressure (SLP) anomalies to the domain average in CTRL (solid) and TORTPD or PDTORT (dashed). The colour of vectors denotes the changes in wind speed (yellow red = increase, blue purple = decrease).

CPD
7, 841–886, 2011

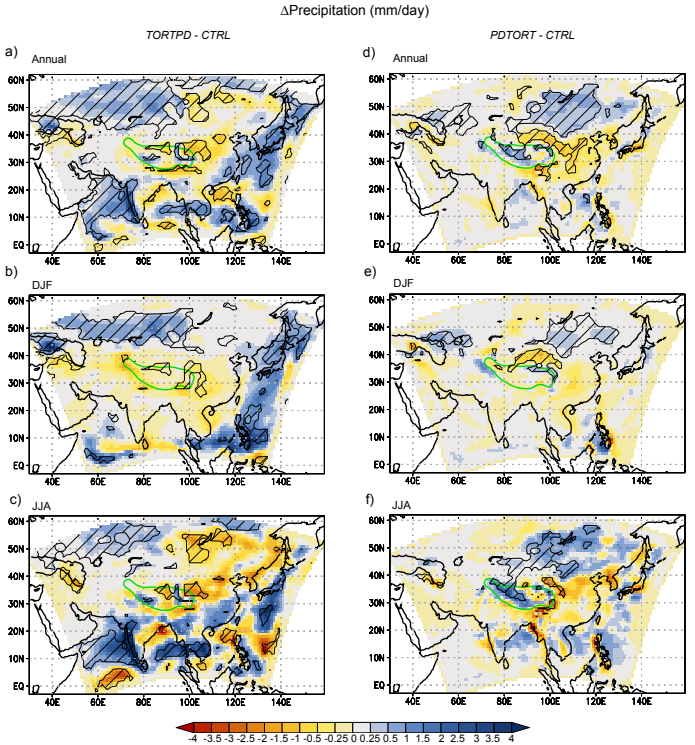

Fig. 11. Precipitation (mm day^{-1}) anomalies of TORTPD and PDTORT runs to the present-day control run (CTRL). **(a, b, c)** TORTPD minus CTRL, **(d, e, f)** PDTORT minus CTRL. **(a, d)** Annual, **(b, e)** winter (DJF), **(c, f)** summer (JJA). The hatched areas have the significant anomalies with a Student's t-test ($p = 0.05$). The green contour denotes the extent of the Tibetan Plateau (>3000 m) in the Tortonian.

CPD
7, 841–886, 2011